Clin Neuroradiol (2018) 28:413–420
DOI 10.1007/s00062-017-0585-9

ORIGINAL ARTICLE

Diffusion Kurtosis as an in vivo Imaging Marker of Early Radiation-Induced Changes in Radiation-Induced Temporal Lobe Necrosis in Nasopharyngeal Carcinoma Patients

Lu Liyan[1] · Wang Si[2] · Wang Qian[2] · Shao Yuhui[3] · Wei Xiaoer[4] · Li Yuehua[4] · Li Wenbin[4]

Received: 21 August 2016 / Accepted: 7 April 2017 / Published online: 26 April 2017

Abstract
Purpose Diffusion kurtosis imaging (DKI), an extension of the popular diffusion tensor imaging (DTI) model, has been applied in clinical studies of brain tissue changes. We explored the value of DKI for the early detection of radiation-induced changes in temporal lobe necrosis (TLN) after radiotherapy (RT) for nasopharyngeal carcinoma (NPC).
Methods A total of 400 patients with NPC were retrospectively enrolled; all participants underwent MRI scans 0–7 days before RT, at 4 weeks during RT, and 1 month after completing RT. DKI-derived kurtosis parameters (mean kurtosis [MK], axial kurtosis [K_a], radial kurtosis [K_r]), and DKI-derived diffusion parameters (fractional anisotropy [FA], mean diffusivity [MD], axial diffusivity [λ_a], radial diffusivity [λ_r]) were assessed in temporal lobe white matter.
Results Analysis was performed for 20 patients with temporal lobe necrosis following long-term follow-up. No brain abnormalities were visible on conventional MRI in any patient at 4 weeks during RT and 1 month after RT. Of all DKI-derived parameters, MK was significantly lower at 1 month after RT than before RT ($P < 0.05$).
Conclusion This study indicates DKI can detect the early presence of relatively subtle RT-induced brain abnormalities before TLN in patients with NPC and may provide a sensitive imaging technique for temporal white matter microstructural abnormalities that are silent on conventional modalities but precede TLN after RT.

Keywords Nasopharyngeal carcinoma · Diffusion kurtosis imaging · Radiotherapy · Temporal lobe · Necrosis

Introduction

Nasopharyngeal carcinoma (NPC) has a unique geographic distribution and varied incidence in different populations; NPC is especially prevalent in southern China [1, 2]. Radiotherapy (RT) remains the mainstay treatment for NPC due to its anatomic complexity and radiosensitivity [3]. As the temporal lobe is in close proximity to the nasopharyngeal cavity, temporal lobe toxicity is one of the limitations on RT for NPC [4]. Moreover, white matter is more vulnerable to irradiation, compared to grey matter [4]. Radiation-induced temporal white matter injury is classified into three stages: the acute period (days to weeks after the initiation of treatment), early delayed period (within 1–6 months of completion of radiation), and late delayed period (after 6 months to many years following therapeutic radiation) [1, 5, 6]. Late delayed injury presents as necrosis and severe functional impairments that are usually permanent and irreversible. However, radiation-induced temporal white matter injury cannot be detected in patients with late delayed injury

✉ Li Yuehua
liyuehua312@163.com

✉ Li Wenbin
lwbprofessor@163.com

1 Department of Radiology, Nanjing First Hospital, Nanjing Medical University, 200016 Nanjing, China

2 Med-X Research Institute, Schools of Biomedical Engineering, Shanghai Jiao Tong University, 200030 Shanghai, China

3 Department of Radiation Oncology, Shanghai Jiao Tong University Affiliated Sixth People's Hospital, 200233 Shanghai, China

4 Department of Radiology, Shanghai Jiao Tong University Affiliated Sixth People's Hospital, No. 600, Yi Shan Road, 200233 Shanghai, China

on routine magnetic resonance imaging (MRI)/computed tomography (CT) examinations during the acute period or early delayed period. Therefore, understanding of the radiation-induced temporal microstructural alterations that occur at the early stage in the white matter of patients with NPC may enable modification of treatment planning and prevent additional severe secondary damage to the brain.

In recent years, diffusion tensor imaging (DTI) has been applied in NPC to detect radiation-induced temporal white matter damage that is not visible using traditional imaging modalities [6–8]. DTI is based on the fundamental assumption that free water diffusion has a Gaussian displacement probability distribution [9]. However, due to the presence of barriers such as cell membranes and organelles that impede the movement of water in most biological tissues [10, 11], the assumption of this Gaussian form is not valid anymore.

Diffusional kurtosis imaging (DKI), as an extension of the popular DTI model [12], characterizes the degree to which diffusion deviates from Gaussian behavior. DKI-derived diffusion parameters (fractional anisotropy [FA], mean diffusivity [MD], axial diffusivity [λ_a], radial diffusivity [λ_r]) and DKI-derived kurtosis parameters (mean kurtosis [MK], axial kurtosis [K_a], radial kurtosis [K_r]) can be used to better understand white matter microstructural changes in the brain [12–15]. DKI has been successfully applied in human studies on aging [16], attention deficit hyperactivity disorder [17], cerebral glioma [18], epilepsy [19, 20] and head and neck cancer [21], as well as in animal models [22], as it can reflect both complex diffusion and kurtosis alterations in the distribution properties of the tissue compartments in white matter.

The aims of the current study were the following: (1) to investigate whether DKI can detect the presence of white matter microstructural changes in the temporal lobe in the early phases following RT for NPC with temporal lobe necrosis and (2) to explore whether DKI provides different and complementary information on radiation-induced changes in temporal white matter.

Patients and Methods

Patients

This study was approved by the Institutional Review Board of Shanghai Jiao Tong University Affiliated Sixth People's Hospital and was conducted in accordance with the Declaration of Helsinki. Written informed consent was obtained from all subjects.

Between June 2008 and July 2010, 400 patients (295 males and 105 females) aged between 18 and 81 (average 53) years old with NPC were studied. All patients had been diagnosed with NPC by biopsy and undergone RT at Shanghai Sixth People's Hospital. In all, 20 patients with stage III–IVa NPC who developed late temporal lobe necrosis following long-term follow-up were retrospectively enrolled in this study.

Patients with intracranial invasion, brain tumor or metastases, diabetes, brain vascular lesions, hypertension, a previous history of radiotherapy, or who were left-handed or had other major medical illness were excluded from the study [6].

Radiotherapy Protocol

Patients were immobilized from the head to shoulders using commercially available thermoplastic masks and individually customized bite blocks. CT images (3 mm slice thickness) were acquired from the top of the vertex to the level of the carina of the trachea. Target volumes were delineated on each axial planning CT slice, based on diagnostic CT images supplemented with diagnostic MRI and/or PET-CT scans. The gross tumor volume (GTV) included the gross extent of the primary disease and involved lymph nodes. Involved lymph nodes were classified as all nodes with a short axis ≥1 cm, nodes with a necrotic center, or nodes that were FDG PET-avid. PTV1 (planning target volume) was defined by adding a 3–5 mm margin to the GTV, depending on the proximity of the GTV to critical structures. PTV2 covered areas at high risk for potential microscopic disease. PTV3 included the clinically negative bilateral cervical lymphatic nodes down to the supraclavicular fossae (elective PTV). Organs at risk were outlined in three dimensions with an estimated planning organ-at-risk volume (PRV) margin of 2–10 mm.

Intensity-modulated radiotherapy plans were generated using the Pinnacle Treatment-Planning System. Irradiation was delivered with 6 MV photon energy using a linear accelerator. The goals were to deliver the prescribed dose to at least 95% of the PTV, and 95% of the prescribed dose to at least 99% of the PTV, while meeting the following normal tissue constraints: spinal cord maximum dose <45 Gy; brain stem maximum dose <54 Gy; temporal lobe maximum dose <54 Gy; eye ball maximum dose <54 Gy; optical nerve maximum dose <54 Gy, mandible maximum dose <70 Gy, dose to 50% of the parotids volume <30 Gy or mean dose <26 Gy, and as low a dose as possible to the lens. We also attempted to keep the volume of tissue receiving >110% of the prescribed dose to <1 cc.

Patients received radiotherapy at a dose of 66 cGy per fraction for a total dose of 1980 cGy to the gross tumor, delivered in 30 fractions over a total period of 6 weeks.

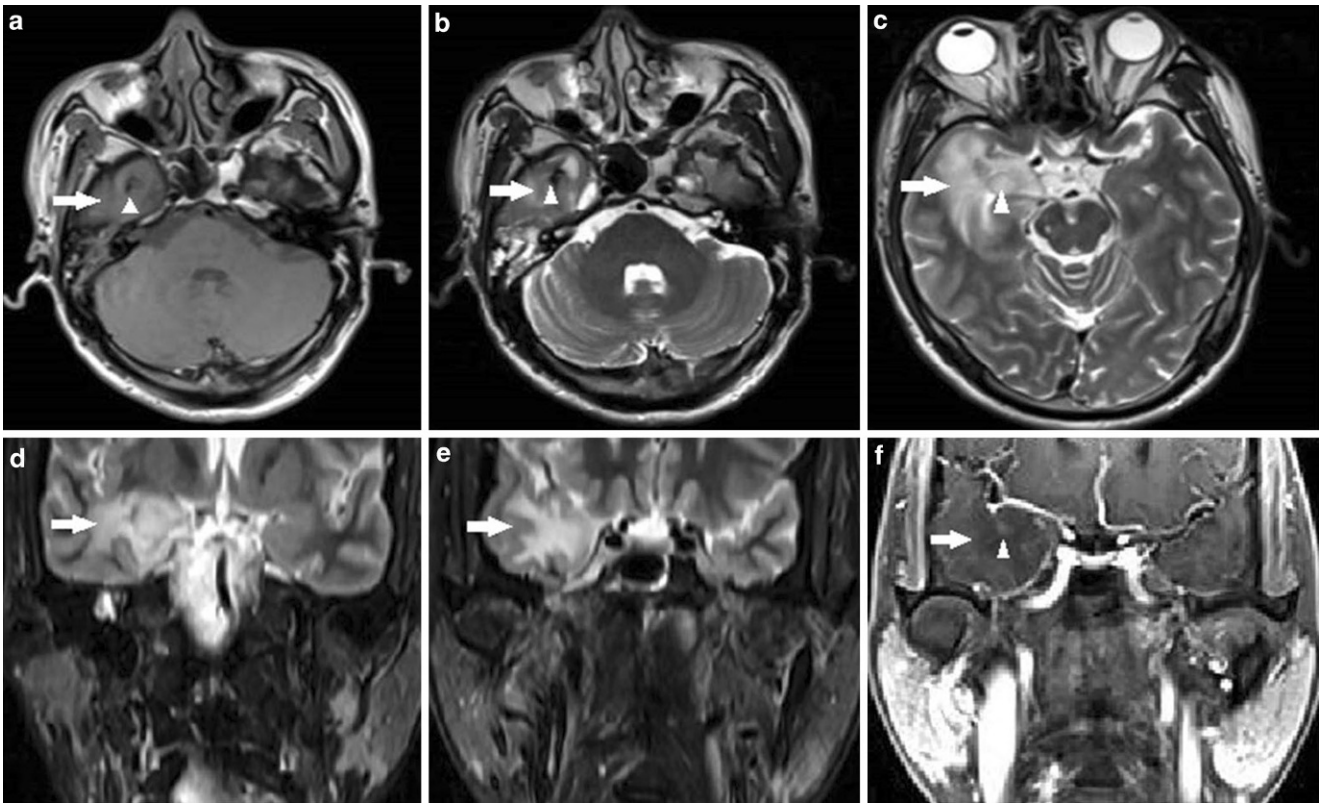

Fig. 1 Magnetic resonance (MR) imaging shows right temporal lobe necrosis in a 40-year-old woman with nasopharyngeal carcinoma at 3.5 years after radiotherapy. **a** Axial T1-weighted image shows right temporal lobe necrosis (*arrow head*) and brain edema (*arrow*); **b** axial T2-weighted image shows right temporal lobe necrosis (*arrow head*) and brain edema (*arrow*); **b**, **c** T2-weighted image shows right temporal lobe necrosis (*arrow head*) and brain edema (*arrow*); **d**, **e** coronal T2-weighted image shows right temporal lobe edema (*arrow*); **f** contrast-enhanced axial T1-weighted image obtained with fat suppression shows contrast enhancement in right temporal lobe necrosis (*arrow head*) and brain edema (*arrow*)

Image Acquisition

MRI was performed using a 3T MR Siemens Trio scanner (Magnetom Verio, Siemens Healthcare, Erlangen, Germany) with a 32 channel head coil at three time points: 0–7 days before initiation of RT, 4 weeks during RT, and 1 month after completion of RT. The protocol included axial T1-weighted images, T2-weighted images, axial DKI, and axial pre- and post-gadolinium T1-weighted images (Gd-DTPA; 0.1 mmol/kg). DKI scanning was acquired at a repetition time of 3700 ms, echo time of 109 ms, 230 mm^2 field of view, 256 × 256 matrix, 2.0 mm slice thickness, and 30% distance factor. The DKI sequence was carried out using *b*-values of 0, 500, 1000, 1500, 2000, and 2500 s/mm^2 in 30 different gradient encoding directions.

MRI Analysis

MRI findings were reviewed by two radiologists and a clinician specializing in head and neck cancers in consensus. The diagnostic criteria of temporal lobe necrosis (TLN) on MRI were as follows:

- White matter lesions (WMLs): areas of finger-like lesions of increased signal intensity in the white matters on T2-weighted images. The size, location and characteristics of signal intensity abnormalities identified on T2-weighted sequences were reviewed.
- Contrast-enhanced lesions: Nodular, rim or heterogeneous signal abnormalities seen on postcontrast, T1-weighted images. The number, size, extent and characteristics of T1-contrast enhancement were reviewed. When the predominant pattern was multiple, small or medium areas of enhancement intermixed with necrotic foci rather than an area of solid enhancement, the features of enhancement include two characteristic patterns – the "Swiss cheese" and "soap bubble". When the predominant pattern was ill-defined and not well demarcated. The enhancement margin was defined as a "spreading wave front".
- Cysts: areas of round or oval, well-defined lesions of increased signal intensity on T2-weighted images, with a thin or imperceptible wall. The size and number of cysts were reviewed.

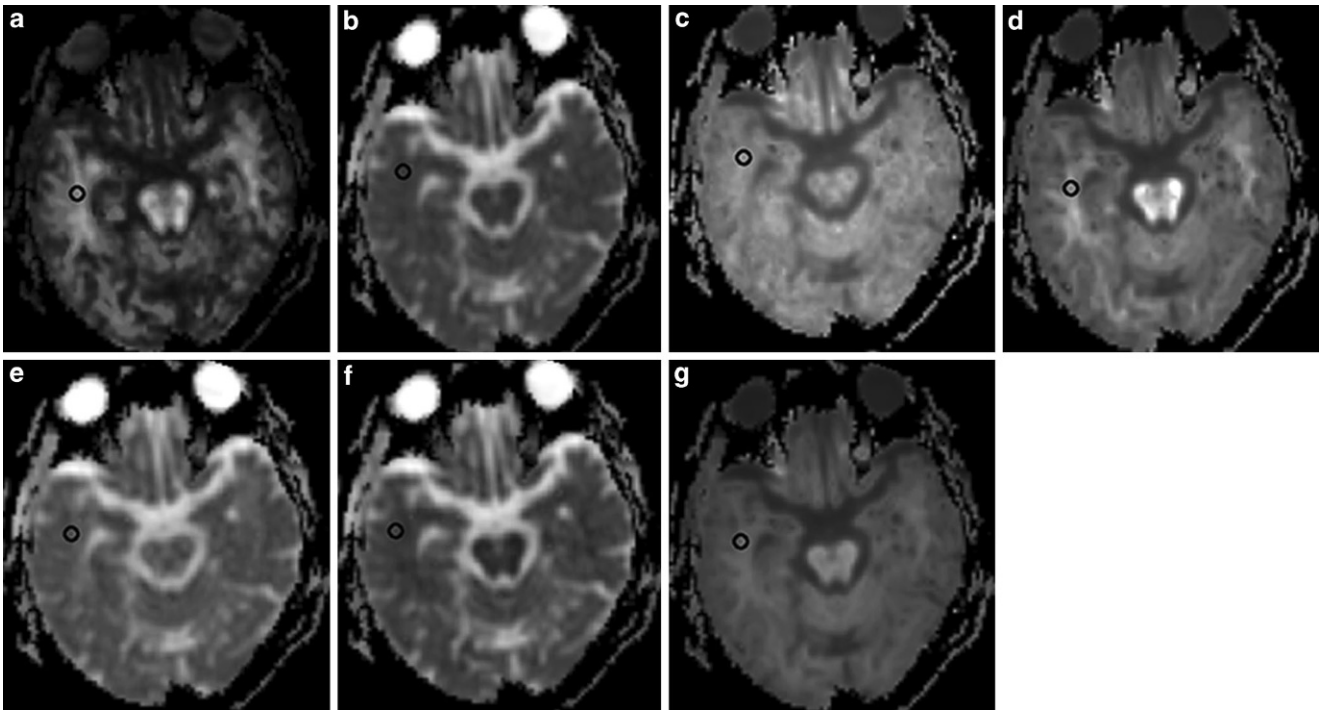

Fig. 2 Axial views of diffusion kurtosis imaging (*DKI*)-derived parametric maps for a 40-year-old woman with nasopharyngeal carcinoma during radiotherapy. **a** Fractional anisotropy (*FA*); **b** mean diffusivity (*MD*); **c** axial kurtosis (*Ka*); **d** radial kurtosis (*Kr*); **e** axial diffusivity (λa); **f** radial diffusivity (λr); **g** mean kurtosis (*MK*)

- Local mass effect: shifting of the brain structures due to the TLN nidus.

An example of temporal lobe necrosis detected by MRI is shown in Fig. 1.

Image Postprocessing and Data Measurement

All image acquisitions were processed using Diffusional Kurtosis Estimator (DKE) [23] and analyzed using MATLAB tools created in-house. All measures (including FA, MD, λ_a, λ_r, MK, K_a, and K_r) were reconstructed following the standard configuration for DKE [23]. Maps of diffusion and perfusion parameters are shown in Figs. 2 and 3. We first identified the slice as close to the spectral location T2-WI anatomy as possible. One uniform circular regions of interest (ROI) was placed in each temporal lobe white matter in the $b = 0$ images in two consecutive sections. A radiologist who was blinded to the patients' identities manually place the ROIs. A code was written to make sure that the diameter for the circular region was 6 mm. The size of the ROIs was about 28 mm^2. Measures were acquired and averaged within each individual ROI. Each lesion was measured twice in two separate sessions spaced 2 weeks apart to ensure reproducibility and showed satisfactory intraobserver agreement with an error of 4.0% coefficient of variance only.

Follow-Up Protocol and Temporal Lobe Necrosis Detected by MRI

Follow-up was calculated from the day of radiation therapy completion to the date of the event or the last follow-up visit. All patients were followed up for the first 3 months, every 3 months for the next 1 years, every 6 months for the next 2 years, and then annually. At each follow-up, disease status and treatment toxicities were assessed by means of head and neck MRI, chest radiography, abdominal ultrasound, physical examination, and, if indicated, whole body bone scanning.

Statistical Analysis

All data are expressed as the mean ± standard deviation values. Statistical analysis was performed using SPSS software version 20.0 (SPSS, Chicago, IL, USA). Analysis of variance (ANOVA) was used to compare the FA, MD, λ_a, λ_r, MK, K_r, and K_a values for the temporal lobe across timepoints. A P-value <0.05 was considered statistically significant for all analyses.

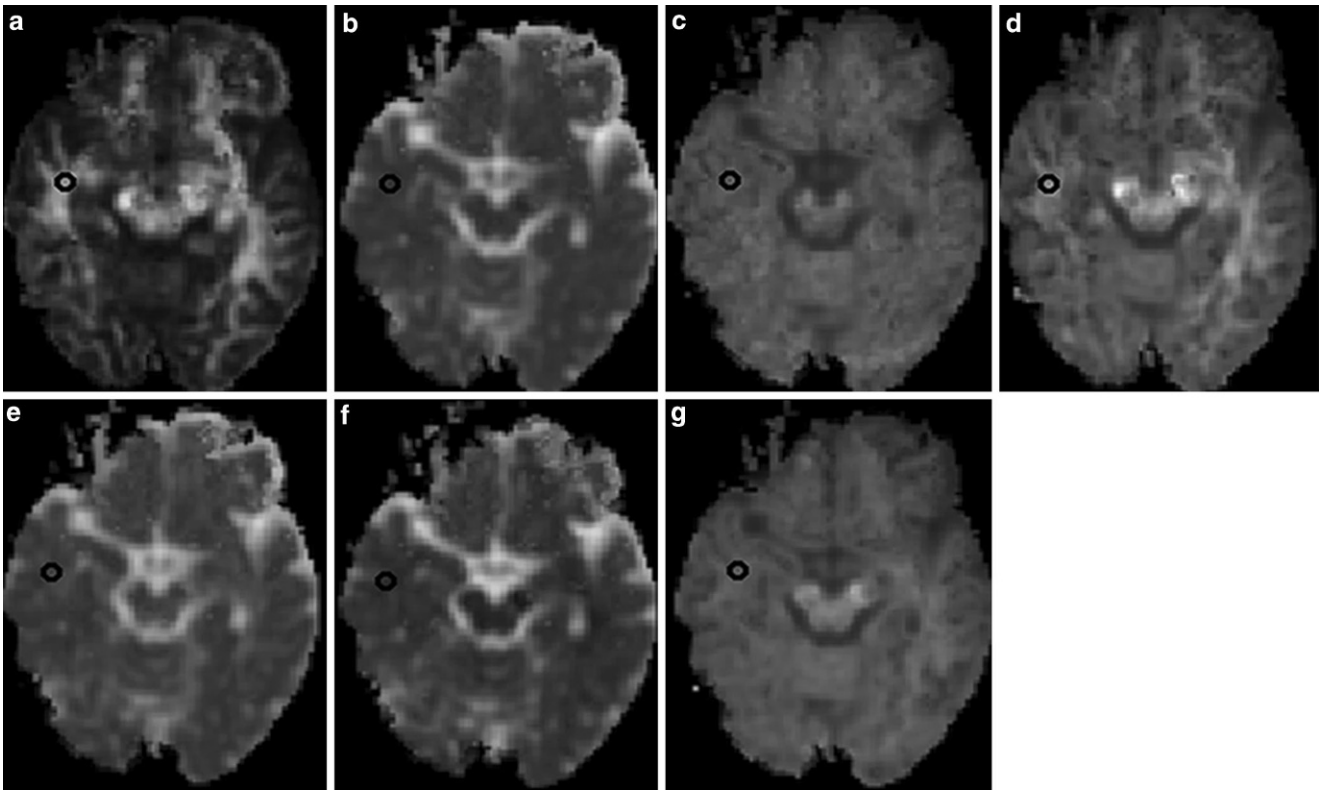

Fig. 3 Axial views of diffusion kurtosis imaging (*DKI*)-derived parametric maps for a 40-year-old woman with nasopharyngeal carcinoma at 1 month after radiotherapy. **a** Fractional anisotropy (*FA*); **b** mean diffusivity (*MD*); **c** axial kurtosis (*Ka*); **d** radial kurtosis (*Kr*); **e** axial diffusivity (λa); **f** radial diffusivity (λr); **g** mean kurtosis (*MK*)

Results

None of the 20 patients displayed radiation-induced lesions on T2-weighted or pre- and post-gadolinium T1-weighted images during and 1 month after radiotherapy for NPC. A total of 20 consecutive patients were analyzed in this study (15 males and 5 females; mean ± standard deviation age 51.2 ± 13.9 years, range 18–76 years; Table 1).

A reduction in λ_a and increase in λ_r for the temporal lobe white matter were observed at 1 month after RT, compared to that before RT; however, these changes were not significant ($P = 0.735$ and 0.109, respectively; Table 2). FA was slightly lower during RT than before RT (Table 2); though this change was not significant ($P = 0.498$). MD tended to be higher at 1 month after RT than before RT (Table 2), but this trend did not reach significance ($P = 0.517$). Ka tended to be higher and Kr tended to be lower at 1 month after RT than before RT, though these differences were not statistically significant ($P = 0.573$ and 0.620, respectively; Table 2). However, MK was significantly lower at 1 month after RT than before RT ($P = 0.006$; Table 2).

Discussion

To our best of our knowledge, this is the first DKI study to evaluate the early diffusion and kurtosis features of temporal lobe white matter following RT in patients with NPC who developed temporal lobe necrosis. This research indicates that DKI can detect radiation-induced abnormalities in the temporal lobe white matter, even when no evidence of changes were evident on conventional MR at earlier phase, in agreement with two reports of an absence of early changes on MRI in patients with late delayed temporal lobe injury [20, 24].

FA, the most commonly used diffusion parameter, measures the directional anisotropy of water molecules [12]. In this group of patients with NPC, although the change was not significant, FA tended to decrease slightly in the early phase after RT (Post-RT), consistent with several previous studies [7–9, 24]. Most DTI investigations of radiation-induced temporal lobe white matter injury have demonstrated that FA decreases and MD increases 1 month after RT in patients with NPC. For example, elevated FA and reduced MD are often observed at 1 month after RT and reverse on long-term follow-up [7, 8]. Previous studies indicated that FA and MD values change dynamically over time, reflecting the dynamic nature of radiation-induced injury [25].

Table 1 Characteristics of the 20 patients with nasopharyngeal cancer whose temporal lobe white matter appeared normal on conventional imaging at 4 weeks during radiotherapy (*RT*) and 1 month after RT

Patient no.	Age (years)	Sex	Clinical tumor staging
1	42	Female	III
2	51	Male	III
3	50	Female	III
4	43	Male	IVa
5	51	Male	III
6	60	Male	III
7	53	Male	IVa
8	41	Male	III
9	42	Male	IVa
10	76	Male	III
11	76	Female	III
12	52	Male	III
13	69	Male	IVa
14	62	Female	III
15	60	Male	III
16	33	Male	III
17	54	Female	III
18	18	Male	III
19	46	Male	III
20	45	Male	III

The decrease in FA is typically attributed to axonal swelling or disruption of ionic homeostasis resulting in an intra- and extracellular water imbalance [25]. In the earlier phases, RT can affect different types of cells within the central nervous system, including neurons, glial cells, and blood vessels [6]. In addition, several factors such as reduced myelination or increased axonal diameter may all contribute to a lower FA value [6, 8]. In this study of patients with NPC, a significant change in MD was not observed after RT which is not in line with a previous study [24]. However this nonsignificant change in MD in this study may be associated with lack of change in overall water diffusion as an integrative change in the cingulum of patients with NPC [26].

The parameter λ_a is believed to be sensitive to axonal injury, whereas λ_r is sensitive to demyelination [6, 27–31]. Song et al. observed that an increase in λ_r with no change in λ_a was indicative of demyelination [27]. In an animal study of irreversible and reversible demyelination, λ_r increased and λ_a and FA significantly decreased due to severe myelin loss; most axons had a small diameter and were unmyelinated [30]. In this study of NPC, λ_a slightly decreased and λ_r slightly increased after RT, consistent with the results of previous studies [6, 20, 28], although the changes in this study were not significant. The reduction in λ_a may be caused by axonal loss or reduced diffusion of water molecules. The elevation in λ_r may be due to an increase in axonal diameter as a result of axonal swelling or demyelination [26]. We suggest that demyelination and axonal injury are the hallmarks of temporal lobe white matter injury after RT in patients with NPC. MD, FA, and λ_r demonstrated very little change between any of the observed time-points in this group of patients, indicating that DKI-derived diffusion parameters have a low sensitivity for temporal lobe microstructural changes.

MK, the average apparent kurtosis along all diffusion encoding directions, quantifies the degree of diffusion restriction or tissue complexity and has been shown to be useful for assessing pathophysiological changes [14, 32, 33]. In the current study, a significant reduction in the MK for the temporal lobe white matter was observed in the patients with NPC at 4 weeks during RT and 1 month after RT. However, in another study [24], the white matter MK values of patients with NPC were significantly lower in the 6-month group and 1-year group. MK may reduce earlier than 6-month based on our results. A decrease in MK suggests a loss of microstructural integrity and the presence of degenerative processes associated with neuronal shrinkage and changes in axonal and myelin density. Ka and Kr measure the kurtoses along the directions parallel and perpendicular to the principal diffusion direction, respectively. The reduced white matter MK and Kr values indicate decreased diffusional heterogeneity, which is likely to be related to reduced cell compartmentalization and an increase in membrane permeability [14, 32–34].

The histological basis of the diffusional kurtosis changes reported here is currently unknown. Several biological processes may underlie the global decline in MK and Kr in white matter following RT, such as myelin breakdown, increased axonal membrane permeability, edema, fiber loss and shortening, as well as a reduction in the density of myelinated axons [35–38], all of which may increase tissue homogeneity and decrease the variability in diffusivity among tissue compartments. The reduction in Ka is likely to be associated with the same biological processes in crossing fibers perpendicular to the principal diffusion direction. However, as cross-sectional changes are also observed in predominantly noncrossing fibers, Ka may additionally be linked to increased homogeneity along the principal diffusion direction, probably due to an increase in extracellular space, which is presumed to have lower heterogeneity than axons and glia [33]. In particular, MK and Kr were reported to indicate more extensive microstructural abnormalities compared with conventional diffusion metrics, such as MD and FA [35].

There are two major limitations to this study. First, the small size of the cohort may have limited the comparison of disease severity and DKI parameters. Second, the underlying tissue microstructure changes revealed by DKI can only be speculated on the basis of limited prior work; further animal studies will be needed to relate the alterations in the

Table 2 Comparisons of DKI-derived diffusion and kurtosis parameters before, during and after radiotherapy in 20 patients with nasopharyngeal cancer

Parameter	Pre-RT		In-RT		Post-RT		P-values		
	Mean	SD	Mean	SD	Mean	SD	P1	P2	P3
FA	0.388	0.027	0.379	0.024	0.375	0.035	NS	NS	NS
MD	0.959	0.011	0.978	0.017	0.987	0.013	NS	NS	NS
λa	1.431	0.081	1.416	0.101	1.406	0.065	NS	NS	NS
λr	0.769	0.010	0.775	0.016	0.779	0.009	NS	NS	NS
MK	1.118	0.116	1.093	0.047	1.018	0.034	NS	0.033	0.006
Ka	0.889	0.004	0.891	0.006	0.891	0.002	NS	NS	NS
Kr	1.284	0.103	1.250	0.088	1.250	0.061	NS	NS	NS

SD standard deviation, *DKI* diffusion kurtosis imaging, *FA* fractional anisotropy, *MD* mean diffusivity, *λa* axial diffusivity, *λr* radial diffusivity, *Ka* axial kurtosis, *Kr* radial kurtosis, *MK* mean kurtosis, *RT* radiotherapy
NS $P > 0.1$, indicating no significant difference between adjacent groups
$P < 0.05$, indicating a significant difference between adjacent groups
P1 Pre-RT vs. In-RT
P2 In-RT vs. Post-RT
P3 Pre-RT vs. Post-RT

DKI parameters suggested by this study with physiological and histological changes. However, our results suggest that assessment of non-Gaussian directional diffusion using DKI may provide a more sensitive indicator of temporal lobe microstructural abnormalities in the early phase after RT in patients with NPC who developed temporal lobe necrosis after long-term follow-up.

Conclusions

This study indicates that DKI has sensitivity for detecting subtle local changes in tissue heterogeneity and may provide a valuable early indicator of regional RT-induced white matter microstructural damage to the temporal lobe in patients with NPC.

Acknowledgements We would like to thank the native English speaking scientists of Elixigen Company (Huntington Beach, CA, USA) for editing our manuscript. This work was supported by the National Natural Science Foundation of China (NSFC; No. 81471656).

Conflict of interest L. Liyan, W. Si, W. Qian, S. Yuhui, W. Xiaoer, L. Yuehua, and L. Wenbin declare that they have no competing interests.

References

1. Shanmugaratnam K, Chan SH, de-Thé G, Goh JE, Khor TH, Simons MJ, Tye CY. Histopathology of nasopharyngeal carcinoma: correlations with epidemiology, survival rates and other biological characteristics. Cancer. 1979;44:1029–44.
2. Jemal A, Bray F, Center MM, Ferlay J, Ward E, Forman D. Global cancer statistics. CA Cancer J Clin. 2011;61:69–90.
3. Zhou GQ, Yu XL, Chen M, Guo R, Lei Y, Sun Y, Mao YP, Liu LZ, Li L, Lin AH, Ma J. Radiation-induced temporal lobe injury for nasopharyngeal carcinoma: a comparison of intensity-modulated radiotherapy and conventional two-dimensional radiotherapy. PLoS One. 2013;8:e67488.
4. Lee AW, Ng SH, Ho JH, Tse VK, Poon YF, Tse CC, Au GK, O SK, Lau WH, Foo WW. Clinical diagnosis of late temporal lobe necrosis following radiation therapy for nasopharyngeal carcinoma. Cancer. 1988;61:1535–42.
5. New P. Radiation injury to the nervous system. Curr Opin Neurol. 2001;14:725–34.
6. Xiong WF, Qiu SJ, Wang HZ, Lv XF. 1H-MR spectroscopy and diffusion tensor imaging of normal-appearing temporal white matter in patients with nasopharyngeal carcinoma after irradiation: initial experience. J Magn Reson Imaging. 2013;37:101–8.
7. Chapman CH, Nagesh V, Sundgren PC, Buchtel H, Chenevert TL, Junck L, Lawrence TS, Tsien CI, Cao Y. Diffusion tensor imaging of normal-appearing white matter as biomarker for radiation-induced late delayed cognitive decline. Int J Radiat Oncol Biol Phys. 2012;82:2033–40.
8. Wang HZ, Qiu SJ, Lv XF, Wang YY, Liang Y, Xiong WF, Ouyang ZB. Diffusion tensor imaging and 1H-MRS study on radiation-induced brain injury after nasopharyngeal carcinoma radiotherapy. Clin Radiol. 2012;67:340–5.
9. Basser PJ, Jones DK. Diffusion-tensor MRI: theory, experimental design and data analysis – a technical review. NMR Biomed. 2002;15:456–67.
10. Tuch DS, Reese TG, Wiegell MR, Wedeen VJ. Diffusion MRI of complex neural architecture. Neuron. 2003;40:885–95.
11. Winston GP. The potential role of novel diffusion imaging techniques in the understanding and treatment of epilepsy. Quant Imaging Med Surg. 2015;5:279–87.
12. Zhu J, Zhuo C, Qin W, Wang D, Ma X, Zhou Y, Yu C. Performances of diffusion kurtosis imaging and diffusion tensor imaging in detecting white matter abnormality in schizophrenia. Neuroimage Clin. 2015;7:170–6.
13. Jensen JH, Helpern JA, Ramani A, Lu H, Kaczynski K. Diffusional kurtosis imaging: the quantification of non-gaussian water diffusion by means of magnetic resonance imaging. Magn Reson Med. 2005;53:1432–40.
14. Jensen JH, Helpern JA. MRI quantification of Non-Gaussian water diffusion by kurtosis analysis. NMR Biomed. 2010;23:698–710.
15. Lu H, Jensen JH, Ramani A, Helpern JA. Three-dimensional characterization of non-gaussian water diffusion in humans using diffusion kurtosis imaging. NMR Biomed. 2006;19:236–47.

16. Falangola MF, Jensen JH, Babb JS, Hu C, Castellanos FX, Di Martino A, Ferris SH, Helpern JA. Age-related Non-Gaussian diffusion patterns in the prefrontal brain. J Magn Reson Imaging. 2008;28:1345–50.
17. Helpern JA, Adisetiyo V, Falangola MF, Hu C, Di Martino A, Williams K, Castellanos FX, Jensen JH. Preliminary evidence of altered gray and white matter microstructural development in the frontal lobe of adolescents with attention-deficit hyperactivity disorder: a diffusional kurtosis imaging study. J Magn Reson Imaging. 2011;33:17–23.
18. Raab P, Hattingen E, Franz K, Zanella FE, Lanfermann H. Cerebral gliomas: diffusional kurtosis imaging analysis of microstructural differences. Radiology. 2010;254:876–81.
19. Zhang Y, Yan X, Gao Y, Xu D, Wu J, Li Y. A preliminary study of epilepsy in children using diffusional kurtosis imaging. Clin Neuroradiol. 2013;23:293–300.
20. Gao Y, Zhang Y, Wong CS, Wu PM, Zhang Z, Gao J, Qiu D, Huang B. Diffusion abnormalities in temporal lobes of children with temporal lobe epilepsy: a preliminary diffusional kurtosis imaging study and comparison with diffusion tensor imaging. NMR Biomed. 2012;25:1369–77.
21. Jansen JF, Stambuk HE, Koutcher JA, Shukla-Dave A. Non-Gaussian analysis of diffusion-weighted MR imaging in head and neck squamous cell carcinoma: a feasibility study. AJNR Am J Neuroradiol. 2010;31:741–8.
22. Cheung MM, Hui ES, Chan KC, Helpern JA, Qi L, Wu EX. Does diffusion kurtosis imaging lead to better neural tissue characterization? A rodent brain maturation study. Neuroimage. 2009;45:386–92.
23. Tabesh A, Jensen JH, Ardekani BA, Helpern JA. Estimation of tensors and tensor-derived measures in diffusional kurtosis imaging. Magn Reson Med. 2011;65:823–36.
24. Wang D, Li YH, Fu J, Wang H. Diffusion kurtosis imaging study on temporal lobe after nasopharyngeal carcinoma radiotherapy. Brain Res. 2016;1648:387–93.
25. Stokum JA, Sours C, Zhuo J, Kane R, Shanmuganathan K, Gullapalli RP. A longitudinal evaluation of diffusion kurtosis imaging in patients with mild traumatic brain injury. Brain Inj. 2015;29:47–57.
26. Kamagata K, Tomiyama H, Motoi Y, Kano M, Abe O, Ito K, Shimoji K, Suzuki M, Hori M, Nakanishi A, Kuwatsuru R, Sasai K, Aoki S, Hattori N. Diffusional kurtosis imaging of cingulate fibers in Parkinson disease: comparison with conventional diffusion tensor imaging. Magn Reson Imaging. 2013;31:1501–6.
27. Song SK, Sun SW, Ramsbottom MJ, Chang C, Russell J, Cross AH. Dysmyelination revealed through MRI as increased radial (but unchanged axial) diffusion of water. Neuroimage. 2002;17:1429–36.
28. Song SK, Sun SW, Ju WK, Lin SJ, Cross AH, Neufeld AH. Diffusion tensor imaging detects and differentiates axon and myelin degeneration in mouse optic nerve after retinal ischemia. Neuroimage. 2003;20:1714–22.
29. Song SK, Yoshino J, Le TQ, Lin SJ, Sun SW, Cross AH, Armstrong RC. Demyelination increases radial diffusivity in corpus callosum of mouse brain. Neuroimage. 2005;26:132–40.
30. Harsan LA, Poulet P, Guignard B, Steibel J, Parizel N, de Sousa PL, Boehm N, Grucker D, Ghandour MS. Brain dysmyelination and recovery assessment by noninvasive in vivo diffusion tensor magnetic resonance imaging. J Neurosci Res. 2006;83:392–402.
31. Ono J, Harada K, Takahashi M, Maeda M, Ikenaka K, Sakurai K, Sakai N, Kagawa T, Fritz-Zieroth B, Nagai T. Differentiation between dysmyelination and demyelination using magnetic resonance diffusional anisotropy. Brain Res. 1995;671:141–8.
32. Lee CY, Tabesh A, Spampinato MV, Helpern JA, Jensen JH, Bonilha L. Diffusional kurtosis imaging reveals a distinctive pattern of microstructural alternations in idiopathic generalized epilepsy. Acta Neurol Scand. 2014;130:148–55.
33. Fieremans E, Novikov DS, Jensen JH, Helpern JA. Monte Carlo study of a two-compartment exchange model of diffusion. NMR Biomed. 2010;23:711–24.
34. Lee CY, Bennett KM, Debbins JP. Sensitivities of statistical distribution model and diffusion kurtosis model in varying microstructural environments: a Monte Carlo study. J Magn Reson. 2013;230:19–26.
35. Coutu JP, Chen JJ, Rosas HD, Salat DH. Non-Gaussian water diffusion in aging white matter. Neurobiol Aging. 2014;35:1412–21.
36. Bartzokis G. Age-related myelin breakdown: a developmental model of cognitive decline and Alzheimer's disease. Neurobiol Aging. 2004;25:5–18.
37. Fazekas F, Kleinert R, Offenbacher H, Schmidt R, Kleinert G, Payer F, Radner H, Lechner H. Pathologic correlates of incidental MRI white matter signal hyperintensities. Neurology. 1993;43:1683–9.
38. Peters A. The effects of normal aging on myelin and nerve fibers: a review. J Neurocytol. 2002;31:581–93.